

Hybrid nano-domain structures of organic-inorganic perovskites from molecule-cage coupling effects

Ping Tuo,¹ Lei Li,² Xiaoxu Wang,^{3,1} Jianhui Chen,⁴ Zhicheng Zhong,^{5,6,*} Bo Xu,^{4,7,†} and Fu-Zhi Dai^{1,‡}

¹*AI for Science Institute, Beijing 100080, China*

²*Frontiers Science Center for Flexible Electronics,*

Xi'an Institute of Flexible Electronics (IFE) and Xi'an Institute of Biomedical Materials & Engineering, Northwestern Polytechnical University, 127 West Youyi Road, Xi'an 710072, China

³*DP Technology, Beijing 100080, China*

⁴*Fujian Science & Technology Innovation Laboratory for Energy Devices of China, Ningde 352100, China*

⁵*Key Laboratory of Magnetic Materials Devices & Zhejiang Province*

Key Laboratory of Magnetic Materials and Application Technology,

Ningbo Institute of Materials Technology and Engineering,

Chinese Academy of Sciences, Ningbo 315201, China

⁶*China Center of Materials Science and Optoelectronics Engineering,*

University of Chinese Academy of Sciences, Beijing 100049, China

⁷*Department of Physics, Laboratory of Computational Materials Physics,*

Jiangxi Normal University, Nanchang 330022, China

In hybrid perovskites, the organic molecules and inorganic frameworks exhibit distinct static and dynamic characteristics. Their coupling will lead to unprecedented phenomena, which have attracted wide research interests. In this paper, we employed Deep Potential molecular dynamics (DPMD), a large-scale MD simulation scheme with DFT accuracy, to study FA/MAPbI₃ hybrid perovskites. A spontaneous hybrid nano-domain behavior, namely multiple molecular rotation nano-domains embedded into a single [PbI₆]⁴⁻ octahedra rotation domain, was firstly discovered at low temperatures. The behavior originates from the interplay between the long range order of molecular rotation and local lattice deformation, and clarifies the puzzling diffraction patterns of FAPbI₃ at low temperatures. Our work provides new insights into the structural characteristics and stability of hybrid perovskite, as well as new ideas for the structural characterization of organic-inorganic coupled systems.

Organic inorganic Hybrid lead iodide perovskite has attracted great research interest due to its surging potential for photovoltaic (PV) applications [1]. Hybrid perovskites have the stoichiometry formula of APbI₃, with A as organic molecule. The structure of a hybrid perovskite consists of organic A-site cations dispersed in an inorganic periodic lattice. The coupling effects between the organic molecules and the inorganic frameworks are concerned in many researches. For example, much attention has been paid to characterize the long range orientation order of A-site molecules [2–8], and it is well-known that the cubic perovskite phase consists of dynamically equilibrated tetragonal polycrystals [9, 10], where the coupling effect prefers stable tetragonal structures locally instead of fully random fluctuations. The coupling effect is not only physically intriguing, resulting in unprecedented phenomena, but also closely related to the stability issue of hybrid perovskites, which is the bottleneck limiting their photovoltaic applications [11].

The static and dynamic characteristics of molecular rotation and the [PbI₆]⁴⁻ octahedra rotation are distinct in time and length scales, yet highly correlated. This leads to great challenge in experiments as well as theoretical

simulations to elucidate their behavior. For example, the $\beta - \gamma$ phase transition of FAPbI₃ (FA=formamidinium, HC(NH₂)₂) was reported to be "re-entrant", where sharp divided diffraction peaks of the high temperature β phase "fuse" into a single wider and weaker peak in the low temperature γ phase [12]. The "re-entrant" transition is a confusing phenomenon, which is unusual and questioned by other researchers [13]. Atomistic simulations are essential approaches to clarify the molecule-cage coupling effects of hybrid perovskites, and to evaluate their influences on the structural characteristics. Due to the long reorientation time of A-site molecules, simulation methods with both high accuracy and high efficiency are desired, which has been made possible recently by machine learning assisted simulations [4, 14–23]. In this work, we adopted the Deep Potential molecular dynamics (DPMD) [24] to study polymorphic transitions of both MAPbI₃ (MA=methylammonium, CH₃NH₃) and FAPbI₃. The temperature dependent phase structures are clarified, where both materials go through phase transitions, from cubic (α) to tetragonal (β), and to orthorhombic (γ), with temperature decreasing. In addition, nano-domain structures resulting from the molecule-cage coupling effect are firstly discovered in γ phases, which will fuzz up the diffraction pattern and lead to difficulties in determining the exact crystal structure of $\gamma - \text{FAPbI}_3$ by experimental methods.

Lattice symmetry. We begin our discussion by clar-

* zhong@nimte.ac.cn

† XuBo@catl-21c.com

‡ daifz@bjaisi.com

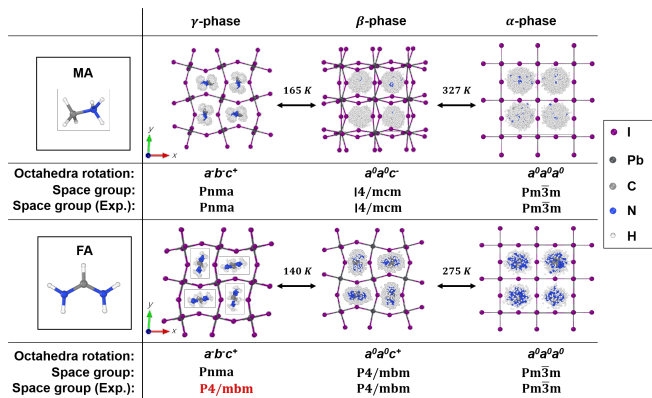


FIG. 1. Overview of the temperature evolution of the perovskite lattice constructed according to symmetry, and time ensembles of organic A cation for MAPbI₃ and FAPbI₃ obtained from MD simulations. Experimental crystal structures and transition temperatures of MAPbI₃ and FAPbI₃ are taken from Weller et al. [25], and Fabini et al. [12] respectively.

ifying the lattice symmetry of each phase. The atomic configurations of the simulated α , β and γ phase of MAPbI₃ and FAPbI₃ are illustrated in Figure 1. The inorganic [PbI₆]⁴⁻ octahedra cages are constructed according to the simulated lattice symmetry, and indicated by their octahedra rotation in Glazer notation [26], while the A-site molecules are illustrated in time ensembles obtained by MD simulations. In the high temperature α phase, A-site molecules rotate almost freely, and the dynamically distorted lattice adopts cubic symmetry (space group Pm3m) on average with equivalent tetragonal distortions [6, 27] and the octahedra rotation $a^0a^0a^0$. In the medium temperature β phase, MAPbI₃ reduces to a body centered tetragonal lattice (space group I4/mcm) with octahedra rotation $a^0a^0c^-$ [28], where the A-site MA molecules still rotate almost freely. In comparison, FAPbI₃ reduces to a primitive tetragonal lattice (space group P4/mbm) with octahedra rotation $a^0a^0c^+$ [29], where the rotation of the A-site FA molecules are confined, especially for the N-N long axis [30]. In the low temperature γ phase, the A-site molecules are almost frozen. Both MAPbI₃ and FAPbI₃ reduces to orthorhombic lattice (space group Pnma) with the C_4 symmetry lost and the octahedra rotation $a^-b^-c^+$ [5, 12, 25, 31, 32]. The frozen A-site molecules form a long range ordered pattern in the γ phases. The relaxed configurations of γ phases are shown in Figure 2(a) and (b). In γ -MAPbI₃, neighboring MA form an orthogonal pattern in the xy plane, with the diagonally neighboring MA ordered ferroelectrically to each other. Thus, each plane should have a net electric polarization, which is canceled out by the antiferroelectric ordering of adjacent planes in the z direction. In comparison, the FA molecules in γ -FAPbI₃ are also ordered orthogonally in the xy plane, while the polar axis of neighboring FA molecules are orthogonal to each other, with a net dipole around zero.

Molecular rotation order. In experiments, the ac-

tivation/deactivation of molecule rotation can be used as an indicator for phase transition [30]. In simulations, the free energy surface (FES) of molecule reorientation can be used to visualize local symmetry, and hence to indicate structural transitions. The on-the-fly probability enhanced sampling (OPES) simulation [33] was adopted to ensure adequate sampling of molecular orientation, especially at lower temperatures. An MA (FA) molecule was randomly selected from a $4 \times 4 \times 4$ supercell, and the polar coordinates of its C-N (N-N) axis were used as collective variables.

The FES of MA and FA rotation in different phases are given in Figure 2(c) and (d), respectively. θ denotes the angle between the C-N axis of MA or the N-N axis of FA and z direction, and ϕ is the angle in the xy plane. In α phase, the FESs show continuous low energy region in the xy plane. In β phase, the FESs exhibit C_4 symmetry in the xy plane. The valleys on the FESs correspond to the orientations lowest in energy, which reveal that face diagonal orientations are preferred by both MA and FA. Notably, in the case of MA, the z direction of the tetragonal cell changes during MD simulations, as shown by the almost degenerate valleys at $\theta \approx 90^\circ$ and $\theta \approx 0^\circ$. When temperature is further lowered through β - γ transition, C_4 symmetry is lost for both MAPbI₃ and FAPbI₃. The sampled orientation of γ -MAPbI₃ is insufficient in comparison with that of γ -FAPbI₃, indicating that the molecule reorientation barrier of γ -MAPbI₃ is higher than that of γ -FAPbI₃, as confirmed and shown in Figure S7 and Figure S8. In γ -FAPbI₃, the θ of the valleys deviate from 90° by $\sim 16.1^\circ$, in agreement with experimental value of around 20° reported by Weber et al. [13].

Hybrid nano-domain structures. We start with the simulated variation of tetragonal parameters $a/c/\sqrt{2}$ and $b/c/\sqrt{2}$ of FAPbI₃ with respect to temperature, as shown in Figure 3. As temperature is lowered through the α - β transition, the tetragonal parameters change from a value around 1 to a value smaller than 1, indicating distortion of the cell from a cubic one to a tetragonal one. When the temperature further decreases to induce the β - γ transition, the parameters $a/c/\sqrt{2}$ and $b/c/\sqrt{2}$ are no longer equal to each other, indicating a tetragonal to orthorhombic transition. The predicted α - β and β - γ transition points are around 300 K and 150 K respectively, within 10 K from the experimental values. Simulated variation of lattice parameters of MAPbI₃ are provided in Figure S4, which also agree well with experiments.

In the work of Fabini et al. [12], a tetragonal cell model was proposed to fit the diffraction patterns of γ -FAPbI₃, and the transition from β to γ phase with decreased temperature was named a "re-entrant" transition. Later, Weber et al. [13] pointed out that the tetragonal model left some peaks unindexed. In our simulations, we also obtained some tetragonal-like γ phase, where $a/c/\sqrt{2}$ and $b/c/\sqrt{2}$ are approximately equal to each other, as illustrated by the circled points in Figure 3(b). These

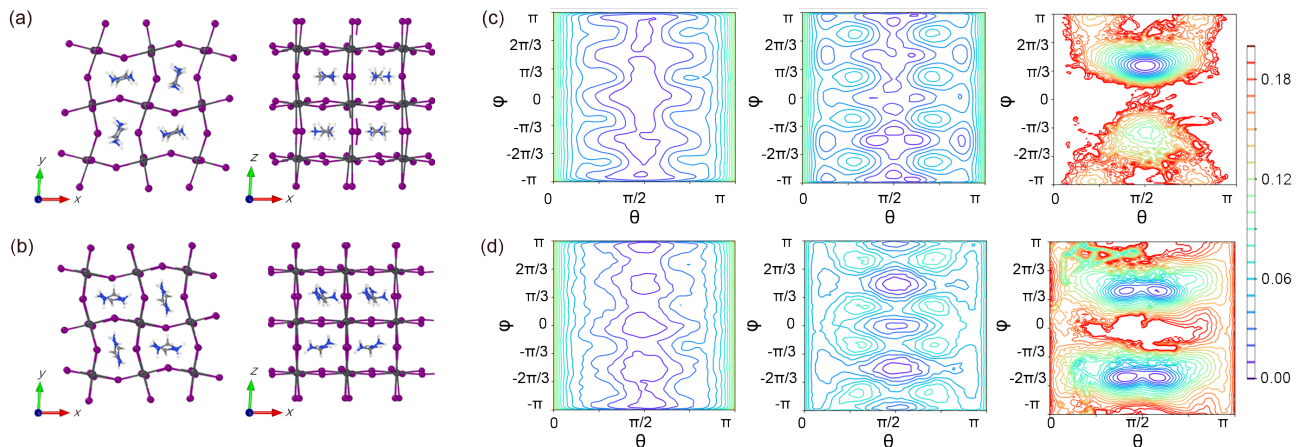


FIG. 2. γ phases of (a) MAPbI₃ and (b) FAPbI₃ viewed from different directions. Free energy surface as a function of polar coordinates of (c) the C-N axis of MA and (d) the N-N axis of FA.

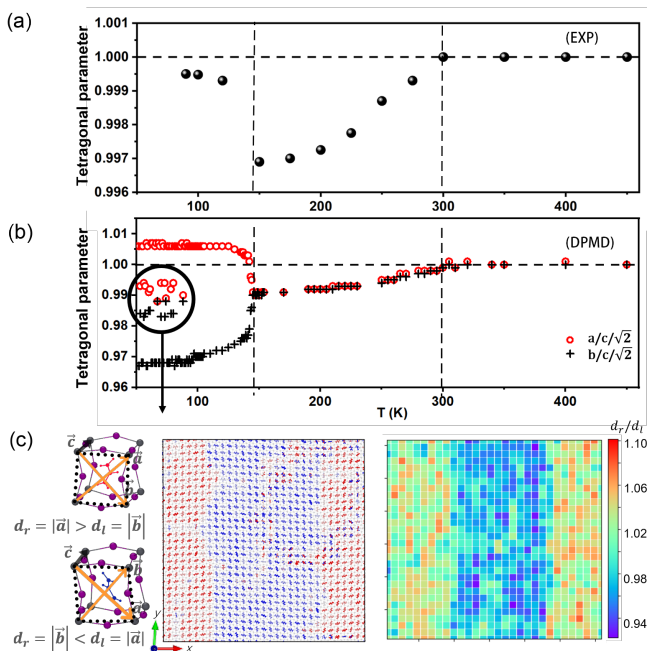


FIG. 3. Phase transitions of FAPbI₃. (a) Tetragonal lattice parameter ratio from synchrotron XRD experiments [12]. (b) Tetragonal lattice parameter ratio simulated by DPMD. The γ phase is orthorhombic with lattice parameters $a \neq b$. For the circled points, $a \approx b$ due to multi-domains in the supercell. (c) Schematic display of the supercell with multi-domains. Multi-domains are colored by the orientation angle of FA molecules and the deformation of cages from a rectangular, respectively. The deformation of cages are indicated by the ratio d_r/d_l in the figure. If $d_r/d_l = 1$, the unit-cell is rectangular in the xy plane; otherwise, the unit-cell is deformed.

tetragonal-like points turn out to be the result of a non-uniform structure with nano-domains, as shown in Figure 3(c). The domain structure is a hybrid one with the molecules rotated to multiple orientations while the octa-

hedra rotation of inorganic framework remains $a^-b^-c^+$. To characterize the domains, we define some parameters here. As explained before, the N-N axis of adjacent FA molecules are approximately parallel to the x axis or the y axis, and orthogonal to each other in the xy plane. We denote the small angle between the N-N axis of horizontal molecules and x axis, or the angle between the N-N axis of vertical molecules and y axis as ψ , and use it to measure the molecular tilting from principle axes. ψ takes a small value within $[-14^\circ, 14^\circ]$, where negative (positive) ψ indicates counter-clock wise (clock wise) small angle rotation relative to the x axis, or clock wise (counter-clock wise) small angle rotation relative to the y axis. In Figure 3(c), a molecule is colored in red if ψ is negative, or colored in blue if ψ is positive. Two distinct domains can be observed in Figure 3(c) according to the small angle rotation relative to x or y axis. Variation of the molecular rotation in space leads to non-uniform local deformation of the lattice. To characterize this effect, we calculated the distribution of the ratio of the length of two diagonals d_r/d_l in space, as illustrated in Figure 3(c). Cells with $d_r/d_l > 1$ are colored in red, while cells with $d_r/d_l < 1$ are colored in blue. As shown in Figure 3(c), domains distinguished by small angle molecular rotation ψ and lattice deformation d_r/d_l are coincident with each other, indicating the coupling nature between molecular rotation and deformation of their surrounding cells. The deformation of different nano-domains compensate each other, makes the supercell in Figure 3(c) rectangular-like in the xy plane, and thus induces nearly equal tetragonal parameters as the circled points in Figure 3(b). The size of the domains are around ~ 5 nm. Similar analyses are also carried out for γ -MAPbI₃ and nano-domains are also found, as given in Figure S4. The approximate characteristic domain size of γ -MAPbI₃ is ~ 2.5 nm, around half the domain size of γ -FAPbI₃.

To understand the mechanism driving the formation of the multi-domains, a modified Ising model with an

auxiliary lattice is constructed, whose Hamiltonian is:

$$H = -J \sum_{\langle ij \rangle} T_i T_j - J' \sum_i T_i T'_i, \quad (1)$$

where pseudo-spins of the main lattice $T_i = +1$ or -1 corresponds to $d_r/d_l > 1$ or < 1 respectively, denoting the local deformation of the cell; pseudo-spins of the auxiliary lattice $T'_i = +1$ or -1 corresponds to $\psi > 0$ or $\psi < 0$, respectively, denoting left or right small angle rotation of the molecule. Since the distances between neighboring molecules are around 6 Å, near the cutoff of the DP model, direct interactions between molecules are negligible. Instead, the molecules interact through the $[\text{PbI}_6]^{4-}$ cages around them. Therefore, the domains can be viewed as a result of two kinds of couplings, the coupling between neighboring cages with coupling constant J , and the coupling between a cage and the molecule within it with coupling constant J' . Standard Monte Carlo simulations were performed by using this model, starting from a randomly initialized lattice to simulate the effect of quenching in experiments. After one billion steps of simulation, the Ising lattice stabilizes at a mosaic pattern with separated "spin-up" and "spin-down" domains (see Figure S6). Characteristic size of the domains decrease with the ratio of the coupling constants J'/J . The reorientation barrier for the molecule is an indicator of the coupling strength. The stronger the coupling is, the higher the barrier is. The reorientation barrier for FA and MA are given in Figure S7, and compared with experimental results. The reorientation barrier for MA in the γ phase is much higher than that for the long N-N axis of FA. Thus, the corresponding coupling constant ratio J'/J of γ -MAPbI₃ is larger than that of γ -FAPbI₃, and the domain size of γ -MAPbI₃ should be smaller than that of γ -FAPbI₃, agreeing with DPMD simulated results. We speculate that the mechanism behind the larger J'/J of γ -MAPbI₃ might be related to the higher hydrogen bonding energy of MA molecule with its surrounding cage. We calculated the hydrogen bonding energy using the method reported by Katrine et al. [34]. The hydrogen bonding energy per molecule of γ -MAPbI₃ is around -0.464 eV, around three times that of γ -FAPbI₃ (-0.144 eV).

To the best of our knowledge, the hybrid nano-domain structure in this work is a new structural phenomenon that has not been reported before. Multiple molecular orientation domains are embedded in a single orthorhombic inorganic domain with uniform $[\text{PbI}_6]^{4-}$ octahedra rotation $a^-b^-c^+$. For MAPbI₃, the inorganic framework transforms from a body-centered structure (β phase with

space group I4/mcm and octahedra rotation $a^0a^0c^-$) to a primitive structure (γ phase with space group Pnma and octahedra rotation $a^-b^-c^+$), as shown in Figure 1. The significant change in the framework will lead to prominent extra diffraction peaks. Therefore, identification of the β and γ phases of MAPbI₃ is not difficult. In contrast, in the case of FAPbI₃, the structure of the $[\text{PbI}_6]^{4-}$ framework of β and γ phases are both primitive structures. As a result, the diffraction pattern will not change substantially. In addition, the nano-domain structure leads to "fused" diffraction peaks due to the uneven interplaner spacing near domain boundaries. "Fused" diffraction patterns were observed in experiments to validate our predictions, as shown in Figure 1 of reference [12], where separated sharp peaks of β phase are "fused" into wide weak peaks in both α and γ phases of FAPbI₃. Even though the temperature is the lowest, diffraction peaks of the γ phase are the most wide and weak, indicating much higher internal stresses in the γ phase.

To sum up, the lattice symmetry and molecule orientation of MAPbI₃ and FAPbI₃ are studied systematically over a wide temperature range of ~ 50 K – 450 K, emphasizing on the low temperature γ phase. Both MAPbI₃ and FAPbI₃ go through polymorphic transitions from cubic (α) to tetragonal (β) and to orthorhombic (γ) phase with decreasing temperature. In the γ phase, neighboring A-site molecules are orthogonal to each other in the xy plane and ordered antiferroelectrically in the z direction. Hybrid nano-domain structures are firstly reported in the γ phases of both perovskites, where nano-domains with multiple molecular rotations are embedded in a single $[\text{PbI}_6]^{4-}$ octahedra rotation domain. The underlying mechanism of the nano-domain structure is the molecule-cage coupling effect where the domain size depends on the coupling strength. This finding provides new insights into the structural characteristics and stability of hybrid perovskites, as well as new ideas for the structural characterization in organic-inorganic coupled systems.

ACKNOWLEDGMENTS

We are grateful to Xifan Wu of Temple University for valuable discussion. This paper was supported by the National Key R&D Program of China (Grants No. 2021YFA0718900), the Key Research Program of Frontier Sciences of CAS (Grant No. ZDBS-LY-SLH008), and the Science Center of the National Science Foundation of China (52088101).

[1] H. Chen, Y. Chen, T. Zhang, X. Liu, X. Wang, Y. Zhao, Advances to high-performance black-phase *FAPbI₃* perovskite for efficient and stable photovoltaics, *Small Structures* 2 (5) (2021) 2000130.

[2] J. Lahnsteiner, G. Kresse, J. Heinen, M. Bokdam, Finite-temperature structure of the *MAPbI₃* perovskite: Comparing density functional approximations and force fields to experiment, *Phys. Rev. Materials* 2 (2018) 073604.

- doi:10.1103/PhysRevMaterials.2.073604.
- [3] M. Bokdam, J. Lahnsteiner, B. Ramberger, T. Schäfer, G. Kresse, [Assessing density functionals using many body theory for hybrid perovskites](#), Phys. Rev. Lett. 119 (2017) 145501. doi:10.1103/PhysRevLett.119.145501. URL <https://link.aps.org/doi/10.1103/PhysRevLett.119.145501>
 - [4] R. Jinnouchi, J. Lahnsteiner, F. Karsai, G. Kresse, M. Bokdam, Phase transitions of hybrid perovskites simulated by machine-learning force fields trained on the fly with bayesian inference, Phys. Rev. Lett. 122 (2019) 225701. doi:10.1103/PhysRevLett.122.225701.
 - [5] J. Lahnsteiner, G. Kresse, A. Kumar, D. Sarma, C. Franchini, M. Bokdam, Room-temperature dynamic correlation between methylammonium molecules in lead-iodine based perovskites: An ab initio molecular dynamics perspective, Physical Review B 94 (21) (2016) 214114.
 - [6] A. N. Beecher, O. E. Semonin, J. M. Skelton, J. M. Frost, M. W. Terban, H. Zhai, A. Alatas, J. S. Owen, A. Walsh, S. J. Billinge, Direct observation of dynamic symmetry breaking above room temperature in methylammonium lead iodide perovskite, ACS Energy Letters 1 (4) (2016) 880–887.
 - [7] A. A. Bakulin, O. Selig, H. J. Bakker, Y. L. Rezus, C. Müller, T. Glaser, R. Lovrincic, Z. Sun, Z. Chen, A. Walsh, et al., Real-time observation of organic cation reorientation in methylammonium lead iodide perovskites, The Journal of Physical Chemistry Letters 6 (18) (2015) 3663–3669.
 - [8] A. Leguy, J. M. Frost, A. P. McMahon, V. G. Sakai, W. Kockelmann, C. Law, X. Li, F. Foglia, A. Walsh, B. C. O’regan, et al., The dynamics of methylammonium ions in hybrid organic-inorganic perovskite solar cells, Nature Communications 6 (1) (2015) 1–11.
 - [9] X.-G. Zhao, G. M. Dalpian, Z. Wang, A. Zunger, Polymorphous nature of cubic halide perovskites, Physical Review B 101 (15) (2020) 155137.
 - [10] O. J. Weber, Structural chemistry of hybrid halide perovskites for thin film photovoltaics, Ph.D. thesis, University of Bath (2018).
 - [11] L. Meng, J. You, Y. Yang, Addressing the stability issue of perovskite solar cells for commercial applications, Nature communications 9 (1) (2018) 1–4.
 - [12] D. H. Fabini, C. C. Stoumpos, G. Laurita, A. Kaltzoglou, A. G. Kontos, P. Falaras, M. G. Kanatzidis, R. Seshadri, Reentrant structural and optical properties and large positive thermal expansion in perovskite formamidinium lead iodide, Angewandte Chemie 128 (49) (2016) 15618–15622.
 - [13] O. J. Weber, D. Ghosh, S. Gaines, P. F. Henry, A. B. Walker, M. S. Islam, M. T. Weller, Phase behavior and polymorphism of formamidinium lead iodide, Chemistry of Materials 30 (11) (2018) 3768–3778.
 - [14] L. Zhang, H. Wang, R. Car, E. Weinan, Phase diagram of a deep potential water model, Physical Review Letters 126 (23) (2021) 236001.
 - [15] J. Wu, Y. Zhang, L. Zhang, S. Liu, Deep learning of accurate force field of ferroelectric HfO_2 , Physical Review B 103 (2) (2021) 024108.
 - [16] L. Tang, Z. Yang, T. Wen, K. Ho, M. Kramer, C. Wang, Short- and medium-range orders in $Al_{90}Tb_{10}$ glass and their relation to the structures of competing crystalline phases, Acta Materialia 204 (2021) 116513. doi:<https://doi.org/10.1016/j.actamat.2020.116513>.
 - [17] F.-Z. Dai, B. Wen, Y. Sun, H. Xiang, Y. Zhou, Theoretical prediction on thermal and mechanical properties of high entropy $(Zr_{0.2}Hf_{0.2}Ti_{0.2}Nb_{0.2}Ta_{0.2})C$ by deep learning potential, Journal of Materials Science & Technology 43 (2020) 168–174.
 - [18] Y. Zhang, C. Gao, Q. Liu, L. Zhang, H. Wang, M. Chen, Warm dense matter simulation via electron temperature dependent deep potential molecular dynamics, Physics of Plasmas 27 (12) (2020) 122704.
 - [19] M. Galib, D. T. Limmer, Reactive uptake of N_2O_5 by atmospheric aerosol is dominated by interfacial processes, Science 371 (2021) 921–925.
 - [20] J. Zeng, L. Cao, M. Xu, T. Zhu, J. Z. H. Zhang, Complex reaction processes in combustion unraveled by neural network-based molecular dynamics simulation, Nat. Commun. 11 (2020) 5713.
 - [21] M. Yang, T. Karmakar, M. Parrinello, Liquid-liquid critical point in phosphorus, Phys. Rev. Lett. 127 (2021) 080603. doi:10.1103/PhysRevLett.127.080603.
 - [22] Y. Wang, J. Wang, A. Hermann, C. Liu, H. Gao, E. Tosatti, H.-T. Wang, D. Xing, J. Sun, Electronically driven 1D cooperative diffusion in a simple cubic crystal, Physical Review X 11 (1) (2021) 011006.
 - [23] H. Wang, X. Guo, L. Zhang, H. Wang, J. Xue, Deep learning inter-atomic potential model for accurate irradiation damage simulations, Applied Physics Letters 114 (24) (2019) 244101.
 - [24] L. Zhang, J. Han, H. Wang, R. Car, W. E, Deep potential molecular dynamics: A scalable model with the accuracy of quantum mechanics, Phys. Rev. Lett. 120 (2018) 143001. doi:10.1103/PhysRevLett.120.143001.
 - [25] M. T. Weller, O. J. Weber, P. F. Henry, A. M. Di Pumpo, T. C. Hansen, Complete structure and cation orientation in the perovskite photovoltaic methylammonium lead iodide between 100 and 352 K, Chemical Communications 51 (20) (2015) 4180–4183.
 - [26] A. M. Glazer, The classification of tilted octahedra in perovskites, Acta Crystallographica Section B: Structural Crystallography and Crystal Chemistry 28 (11) (1972) 3384–3392.
 - [27] Schwarzenbach, D., Acta crystallographica section A: Foundations of crystallography, Acta Cryst Sect A (2008).
 - [28] Y. Ren, I. W. Oswald, X. Wang, G. T. McCandless, J. Y. Chan, Orientation of organic cations in hybrid inorganic-organic perovskite $CH_3NH_3PbI_3$ from subatomic resolution single crystal neutron diffraction structural studies, Crystal Growth & Design 16 (5) (2016) 2945–2951.
 - [29] S. Sun, Z. Deng, Y. Wu, F. Wei, F. H. Isikgor, F. Brivio, M. W. Gaultois, J. Ouyang, P. D. Bristowe, A. K. Cheetham, et al., Variable temperature and high-pressure crystal chemistry of perovskite formamidinium lead iodide: a single crystal x-ray diffraction and computational study, Chemical Communications 53 (54) (2017) 7537–7540.
 - [30] D. H. Fabini, T. A. Siaw, C. C. Stoumpos, G. Laurita, D. Olds, K. Page, J. G. Hu, M. G. Kanatzidis, S. Han, R. Seshadri, Universal dynamics of molecular reorientation in hybrid lead iodide perovskites, Journal of the American Chemical Society 139 (46) (2017) 16875–16884.
 - [31] I. Swainson, R. Hammond, C. Soullière, O. Knop, W. Massa, Phase transitions in the perovskite methylammonium lead bromide, $CH_3NH_3PbBr_3$, Journal of Solid State Chemistry 176 (1) (2003) 97–104.

- [32] O. Weber, B. Charles, M. Weller, Phase behaviour and composition in the formamidinium-methylammonium hybrid lead iodide perovskite solid solution, *Journal of Materials Chemistry A* 4 (40) (2016) 15375–15382.
- [33] M. Invernizzi, P. M. Piaggi, M. Parrinello, Unified approach to enhanced sampling, *Phys. Rev. X* 10 (2020) 041034. doi:10.1103/PhysRevX.10.041034.
- [34] K. L. Svane, A. C. Forse, C. P. Grey, G. Kieslich, A. K. Cheetham, A. Walsh, K. T. Butler, How strong is the hydrogen bond in hybrid perovskites?, *The Journal of Physical Chemistry Letters* 8 (24) (2017) 6154–6159.